EUROPEAN ORGANIZATION FOR NUCLEAR RESEARCH (CERN)

CERN-EP-2022-219
2022/12/03

CMS-HIN-21-003

Measurements of azimuthal anisotropy of nonprompt D^0 mesons in PbPb collisions at $\sqrt{s_{NN}} = 5.02\,\text{TeV}$

The CMS Collaboration

Abstract

Measurements of the elliptic (v_2) and triangular (v_3) azimuthal anisotropy coefficients are presented for D^0 mesons produced in b hadron decays (nonprompt D^0 mesons) in lead-lead collisions at $\sqrt{s_{NN}} = 5.02\,\text{TeV}$. The results are compared with previously published charm meson anisotropies measured using prompt D^0 mesons. The data were collected with the CMS detector in 2018 with an integrated luminosity of $0.58\,\text{nb}^{-1}$. Azimuthal anisotropy is sensitive to the interactions of quarks with the hot and dense medium created in heavy ion collisions. Comparing results for prompt and nonprompt D^0 mesons can assist in understanding the mass dependence of these interactions. The nonprompt results show lower magnitudes of v_2 and v_3 and weaker dependences on the meson transverse momentum and collision centrality than those found for prompt D^0 mesons. By comparing to theoretical predictions, the results imply that there is a mass hierarchy of quark interactions with the medium.

Submitted to Physics Letters B

1 Introduction

In ultra-relativistic heavy ion collisions, cold nuclear matter transforms into a state of strongly coupled matter, called the quark-gluon plasma (QGP) [1–4]. One of the main features of the QGP is the collective motion of its constituents. This collectivity can be quantified by measuring the momentum anisotropy of the particles that emerge from the collision. In the plane perpendicular to the beam axis (transverse plane), this anisotropy results from the initial transverse spatial anisotropy of the colliding system. To quantify this effect, azimuthal (Fourier) coefficients of order n, $v_{\mathrm{n}} = \langle \cos[n(\phi - \Psi_n)] \rangle$ can be used, where ϕ is the single-particle azimuthal angle and Ψ_n is the first angle where the n-th harmonic component has its maximum multiplicity [5, 6]. The measured v_{n} values for low-momentum light hadrons can be described by relativistic hydrodynamics, and this behavior is known as collective anisotropic flow [7–9]. The second Fourier coefficient, v_2 (referred to as elliptic flow), arises from the combined effects of the elongated shape and the event-by-event fluctuations of the overlap region of the colliding nuclei [10]. The third coefficient, v_3 (referred to as triangular flow), is predominantly due to the fluctuations.

Because of their large mass, bottom (b) and charm (c) quarks are produced at the earliest stage of the collision [11], but their azimuthal distributions can be affected by their interaction with the medium as they travel through the QGP [12]. At low transverse momentum (p_{T}), it is believed that heavy quarks thermalize and, therefore, they should follow the motion of the light flavor particles [13]. In the high p_{T} region, the flow could be caused by the path length dependence of parton energy loss [14, 15]. Hence, studying the collectivity of heavy quarks in heavy ion collisions can provide important inputs for understanding the properties of the QGP. Significant v_2 and v_3 coefficients of charm hadrons in lead-lead (PbPb) collisions have already been measured at the CERN LHC, proving that heavy quarks exhibit collective flow [16–21]. An early measurement by the CMS Collaboration of the elliptic flow of J/ψ from b hadron decays was consistent with zero, albeit with large uncertainties [22]. Recently, the ALICE Collaboration measured the v_2 of electrons from b hadron decays [23], and the ATLAS Collaboration measured both v_2 and v_3 of muons from b hadron decays [19]. These results show a nonzero elliptic flow for b hadrons, as well as clear mass ordering, with smaller measured values of Fourier coefficients than those found for lighter quarks. With respect to these J/ψ or lepton measurements, the b $\rightarrow$ D^0 channel is a promising laboratory because of its lower p_{T} coverage and large branching ratio ($\sim$70%). In addition, because of its large mass, the D^0 momentum is more closely correlated with the b quark momentum than is the case for leptons.

In this Letter, the first v_2 and v_3 measurements of D^0 mesons from b hadron decay (nonprompt D^0 mesons) in large collision systems are reported, using PbPb collisions at a center-of-mass energy per nucleon pair of $\sqrt{s_{\mathrm{NN}}} = 5.02$ TeV. Results for D^0 mesons in the rapidity range $|y| < 1$ are shown as a function of their p_{T}, spanning 1–30 GeV/c, and in three classes of PbPb centrality: 0–10%, 10–30%, and 30–50%. These centrality percentages represent the fraction of the total inelastic hadronic cross section, with 0% corresponding to full overlap of the two colliding nuclei. The broad range in p_{T} enables a comprehensive study of different flow generation mechanisms. The results are compared with azimuthal anisotropy measurements of D^0 mesons that do not come from b hadron decays (prompt D^0 mesons) [18], as well as with theoretical predictions. Tabulated results are provided in the HEPData record for this analysis [24].

2 Experimental setup and data sample

The CMS apparatus [25] is a multipurpose, nearly hermetic detector, designed to trigger on [26, 27] and identify electrons, muons, photons, and (charged and neutral) hadrons [28–30]. A global algorithm [31] aims to reconstruct all individual particles in an event, combining information provided by the all-silicon inner tracker and by the crystal electromagnetic and brass-scintillator hadron calorimeters, operating inside a 3.8 T superconducting solenoid, with data from the gas-ionization muon detectors embedded in the flux-return yoke outside the solenoid. The forward hadron (HF) calorimeter uses steel as an absorber and quartz fibers as the sensitive material. The two halves of the HF are located 11.2 m from the interaction region, one on each end, and together they provide coverage in the pseudorapidity range $3.0 < |\eta| < 5.2$. The HF calorimeters are subdivided into "towers" with $\Delta\eta \times \Delta\phi = 0.175 \times 0.175$, and energy deposited in a tower is treated as a detected hadron in this analysis. They serve as luminosity monitors and the total energy deposited in both HF calorimeters is used for centrality determination [32]. Events are filtered using a two-tiered trigger system. The first level, composed of custom hardware processors, uses information from the calorimeters and muon detectors [26]. The second level, known as the high-level trigger [27], consists of a farm of processors running a version of the full event reconstruction software.

The data analyzed in this Letter consist of minimum bias (MB) PbPb events corresponding to an integrated luminosity of $0.58\,\mathrm{nb}^{-1}$ [33, 34]. The MB selection requires signals above readout thresholds in the range of ∼6–12 GeV on both sides of the HF calorimeters [27]. The events are further filtered to remove background events (beam-gas interactions and nonhadronic collisions) by applying the procedure described in Ref. [35]. The final results include only events with at least one vertex associated with two or more tracks (primary vertex) within 15 cm from the nominal interaction point along the beam direction, and at least two towers with energy larger or equal to 4 GeV in each of the HF detectors. Finally, in order to suppress the contamination from events with multiple ion collisions, the shapes of the clusters in the pixel part of the inner tracker are required to be compatible with those expected in single PbPb collisions.

Simulated events from Monte Carlo (MC) generators are used to study the kinematics of D^0 mesons in PbPb collisions. The D^0 mesons are generated with PYTHIA 8.212 [36], tune CP5 [37], while their decays are modeled with EVTGEN 1.3 [38]. Both prompt and nonprompt D^0 samples are produced. The decay products of the D^0 mesons are then embedded into MB events generated using HYDJET 1.9 [39]. The response of the CMS detector to these combined events is simulated with GEANT4 [40].

3 Analysis procedure

Inclusive (both prompt and nonprompt) D^0 and $\overline{\mathrm{D}}^0$ meson candidates are reconstructed via their decay channels: $\mathrm{D}^0 \to \pi^+ + \mathrm{K}^-$ and $\overline{\mathrm{D}}^0 \to \pi^- + \mathrm{K}^+$. Both D^0 and $\overline{\mathrm{D}}^0$ are referred to as D^0 in this Letter. All tracks used in the analysis have $p_\mathrm{T} > 1\,\mathrm{GeV}/c$ and $|\eta| < 1.2$. To ensure the best track quality, only tracks that satisfy high purity [30] criteria are considered. In addition, the relative uncertainty in the track p_T measurement is required to be less than 10%. The number of hits along the track trajectory in the tracker must be greater or equal to 11. The χ^2 of the track fit divided by the total number of degrees of freedom of the fit, and also divided by the total number of tracker layers having a hit along the track path, must be less than 0.18. Candidates are formed by combining pairs of tracks from oppositely-charged particles and requiring an invariant mass (m_inv) within a $\pm 200\,\mathrm{MeV}/c^2$ window of the world-average D^0 meson mass of $1865\,\mathrm{MeV}/c^2$ [41]. Since no particle identification is available, both

possible particle assignments (pion and kaon) are considered for each pair of selected candidate decay tracks.

Further selection is done by applying a boosted decision tree (BDT) algorithm implemented using the TMVA package [42]. For the BDT training, the signal candidates are taken from the simulated events in which reconstructed D^0 mesons are required to match the generated nonprompt D^0 particles. The background training sample consists of two components combined together: combinatorial background and prompt D^0 production. The combinatorial background sample is composed of D^0 candidates reconstructed from data whose mass is three to six standard deviations away from the nominal D^0 meson mass ($\sim$1.795–1.830 and $\sim$1.900–1.935 GeV/c^2). The prompt D^0 meson component of the background sample consists of D^0 candidates that correspond to simulated prompt D^0 mesons in the MC events. In this way, the training is optimized to favor the D^0 mesons produced in b hadron decays. Training is performed separately for each p_T range and centrality class. The variables related to D^0 mesons used to discriminate the signal from the background are: χ^2 probability for the D^0 vertex fit, the distance between the D^0 and primary vertices and its significance, as well as the angle between the momentum of the D^0 meson candidate and the line connecting the primary and D^0 vertices (pointing angle). In addition, related to the decay products of the D^0 meson candidate, the variables used are: the significance of the distances of closest approach (DCA) to the primary vertex (both along and perpendicular to the beam direction), and the number of hits assigned to a particular track. These variables are chosen by analyzing their importance in the decision tree and the correlation matrix among all variables. The BDT cut is optimized to correspond to the maximal nonprompt D^0 mesons signal significance for each analysis bin. Each D^0 candidate is weighted by a correction factor, defined as the product of the acceptance and selection efficiencies as functions of p_T and centrality. This factor is calculated from the MC sample using the ratio of the number of reconstructed D^0 mesons (that satisfy selection criteria) to the total number of generated nonprompt D^0 mesons in a certain kinematic range. Potential discrepancies between data and simulated p_T spectra could lead to an inaccuracy in the correction factor. Therefore, before performing this calculation, the p_T spectrum of D^0 mesons in the simulation is weighted to match that in the data.

The measurement of inclusive D^0 meson v_n coefficients employs the scalar-product (SP) method [43] used in previous CMS publications for prompt D^0 mesons [17, 18].

In this method, the v_n coefficients of all D^0 candidates ($v_\mathrm{n}^{\mathrm{sig+bkg}}$) are determined using

$$v_\mathrm{n}\{\mathrm{SP}\} \equiv \frac{\langle Q_n^{\mathrm{D}^0} Q_{n\mathrm{A}}^* \rangle}{\sqrt{\frac{\langle Q_{n\mathrm{A}} Q_{n\mathrm{B}}^* \rangle \langle Q_{n\mathrm{A}} Q_{n\mathrm{C}}^* \rangle}{\langle Q_{n\mathrm{B}} Q_{n\mathrm{C}}^* \rangle}}}, \tag{1}$$

where the Q-vectors are defined as $Q_n \equiv \sum_{j=1} w_j e^{in\phi_j}$, the asterisk symbol (*) means complex conjugation, and the subscripts A, B, and C refer to different subevents. In each event, the sum for $Q_{n\mathrm{A}}$ and $Q_{n\mathrm{B}}$ is over all hadrons detected in HF which are above a threshold energy, while the sum for $Q_{n\mathrm{C}}$ includes all reconstructed tracks above a p_T threshold. The $Q_n^{\mathrm{D}^0}$ signifies the flow vector of a D^0 meson candidate within a particular kinematic range. The weight w_j is a dimensionless quantity and corresponds to the energy deposited in the HF tower in GeV, or to the track p_T in GeV/c, at azimuthal angle ϕ_j, or $w_j = 1$ in the case of D^0 meson candidates. The subevent A (B) uses the negative (positive) side of the HF when the D^0 meson candidate is at positive pseudorapidity, and vice versa. This choice of subevents avoids autocorrelations and results in an η gap of at least three units between the D^0 meson daughters and particles from the underlying subevent, thereby suppressing short-range correlations. Flattening and recentering

procedures are applied to the Q-vectors related to HF and the tracker, for removing detector acceptance effects [44, 45]. The averages $\langle Q_{n\mathrm{A}} Q^*_{n\mathrm{B}} \rangle$, $\langle Q_{n\mathrm{A}} Q^*_{n\mathrm{C}} \rangle$, and $\langle Q_{n\mathrm{B}} Q^*_{n\mathrm{C}} \rangle$ are found by considering all selected events, while the average $\langle Q_n^{\mathrm{D}^0} Q^*_{n\mathrm{A}} \rangle$ includes all D^0 meson candidates in all selected events.

To extract the inclusive D^0 meson flow harmonics, the individual D^0 candidates are divided into bins of their flow vector SPs (i.e., Eq. (1) but not averaged over all D^0 candidates). A separate mass spectrum is generated in each of these SP bins and an invariant mass fit is performed to get the SP distribution of the D^0 signal. The inclusive D^0 v_n values can be obtained by:

$$v_\mathrm{n}^{\mathrm{D}^0} = \frac{\sum v_\mathrm{n}^i Y_i}{\sum Y_i}, \tag{2}$$

where v_n^i is the center of the i-th SP bin, and the Y_i is the D^0 yield in the same bin.

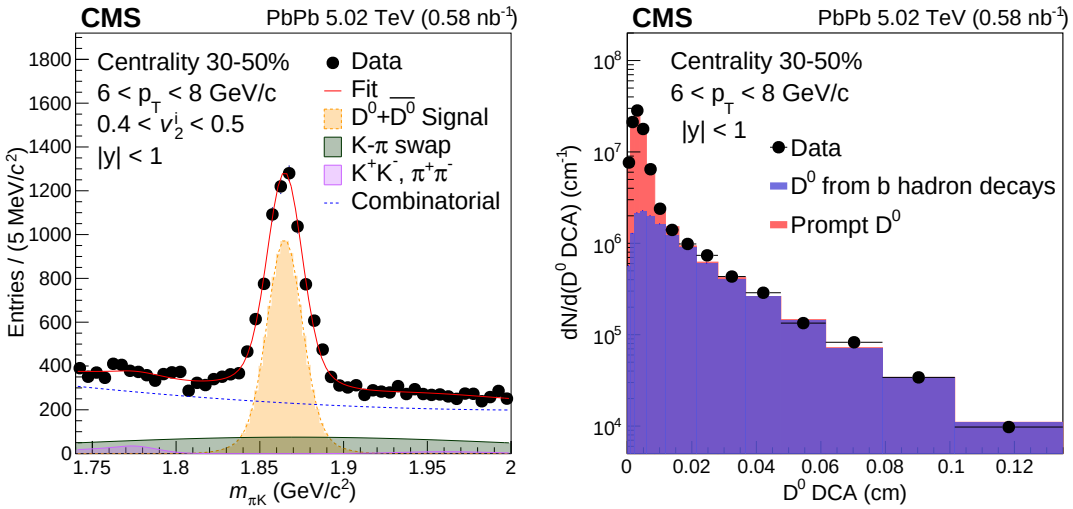

Figure 1: An example of the fit to the invariant mass spectrum (left panel) and an example of the template fit of the inclusive D^0 meson yields, extracted as a function of DCA (right panel). The former fit is used for determining the total D^0 yields and the latter for determining the fraction of nonprompt D^0 mesons.

The m_inv distributions are fitted with five components, as shown in Fig. 1: the sum of two Gaussian functions with the same mean but different widths for the D^0 signal, $S(m_\mathrm{inv})$; an additional Gaussian function to describe the invariant mass shape of those D^0 candidates that were given an incorrect mass assignment when swapping the pion and kaon designations, $SW(m_\mathrm{inv})$; two Crystal Ball functions [46] to describe the processes $\mathrm{D}^0 \to \pi^+\pi^-$ ($S(m_{\pi^+\pi^-})$) and $\mathrm{D}^0 \to \mathrm{K}^+\mathrm{K}^-$ ($S(m_{\mathrm{K}^+\mathrm{K}^-})$); and a third-order polynomial to model the combinatorial background, $Bkg(m_\mathrm{inv})$. The contributions from the processes $\mathrm{D}^0 \to \pi^+\pi^-$ and $\mathrm{D}^0 \to \mathrm{K}^+\mathrm{K}^-$ are also resulting from using an incorrect K or π assignment. The ratio between the $S(m_\mathrm{inv})$ and $SW(m_\mathrm{inv})$ function yields is fixed according to values obtained from simulated events. The widths of the $S(m_\mathrm{inv})$, $SW(m_\mathrm{inv})$, and Crystal Ball functions are initialized by results obtained from simulation studies. They are allowed to vary with a single scale factor common to all three functions during the fit to data.

The fit of the invariant mass spectrum gives the yield for inclusive D^0 mesons. For the extraction of the two individual components (prompt and nonprompt), a similar procedure as in Refs. [47, 48] is followed. Distributions of the DCA between the D^0 meson momentum vector

and primary vertex are fitted with a linear combination of prompt and nonprompt D^0 DCA templates obtained from MC in each bin of p_T, centrality, and v_n^i. The widths of the simulated distributions are scaled to match the data. The same scale factor is chosen for both prompt and nonprompt distributions by minimizing the χ^2 of the template fit.

The left panel of Fig. 1 shows an example of a fit to the mass spectrum for D^0 candidates in the p_T interval 6–8 GeV/c for the centrality class 30–50% and the SP range $0.4 < v_n^i < 0.5$. The right panel shows an example of the template fit of the inclusive D^0 meson yields, extracted as a function of DCA in the same D^0 kinematic region, but averaged over all v_n.

4 Systematic uncertainties

Systematic uncertainties are estimated by varying the conditions and procedures of the v_n measurements. In the remaining discussion, numbers in parentheses give the absolute differences in v_n between the nominal and the alternative analyses. In the fit to m_{inv}, the functional form of the combinatorial background was varied using a second-order polynomial and an exponential function (0.002 to 0.012). For the signal mass shape systematic check, a triple-Gaussian function is used and negligible differences are observed. The effect of the efficiency is studied by changing the efficiency correction values. In this alternative approach, the efficiency is based solely on simulation and does not consider any potential differences between the MC and data spectra (less than 0.0005). The systematic uncertainty from the determination of the nonprompt D^0 meson fraction is evaluated by performing the template fit using an alternative variable, the DCA significance (DCA/(DCA uncertainty)). In the case of DCA significance, the MC/data discrepancy is partially cancelled out by dividing DCA by its uncertainty. However, as DCA significance arises from the D^0 reconstruction, the widths of the distributions cannot be scaled to further match the data in the same way it was done for DCA. The difference in results between the DCA and DCA significance template fits is quoted as a systematic uncertainty. The largest uncertainty comes from this variation of the template fit (0.006 to 0.013). Systematic uncertainties in the BDT selection of the D^0 candidates are evaluated by studying MC samples. The difference between applying BDT selections and not applying those criteria is taken as the systematic uncertainty (0.001 to 0.006). The total systematic uncertainty is obtained by adding individual uncertainties in quadrature.

5 Results

The nonprompt D^0 meson flow harmonics are presented in Fig. 2 together with values for prompt D^0 mesons from Ref. [18]. The results show nonzero values of elliptic flow of b mesons. The v_2 coefficient in the case of b hadron daughters has its maximum value at p_T of $\sim$5 GeV/c and is significantly lower than in the prompt D^0 meson case. This difference becomes more pronounced going from central to peripheral collisions. The observed mass ordering of collective flow agrees with the relation between charm and light quarks, where lighter particles exhibit higher flow. Measurements also suggest an increase of v_2 towards peripheral collisions, as in the case of light hadrons. This observation agrees with the paradigm of flow as a consequence of initial space anisotropy [10]. The elliptic flow of nonprompt D^0 mesons is found to be of the same magnitude as what the ATLAS Collaboration observed for nonprompt muons in the range $p_T > 10$ GeV/c [19].

The nonprompt v_3 coefficient results have large statistical uncertainties so that neither the p_T nor the centrality dependence can be determined. However, an indication of a nonzero value is seen in the $4 < p_T < 6$ GeV/c range for all centralities. As was the case for v_2, the triangular

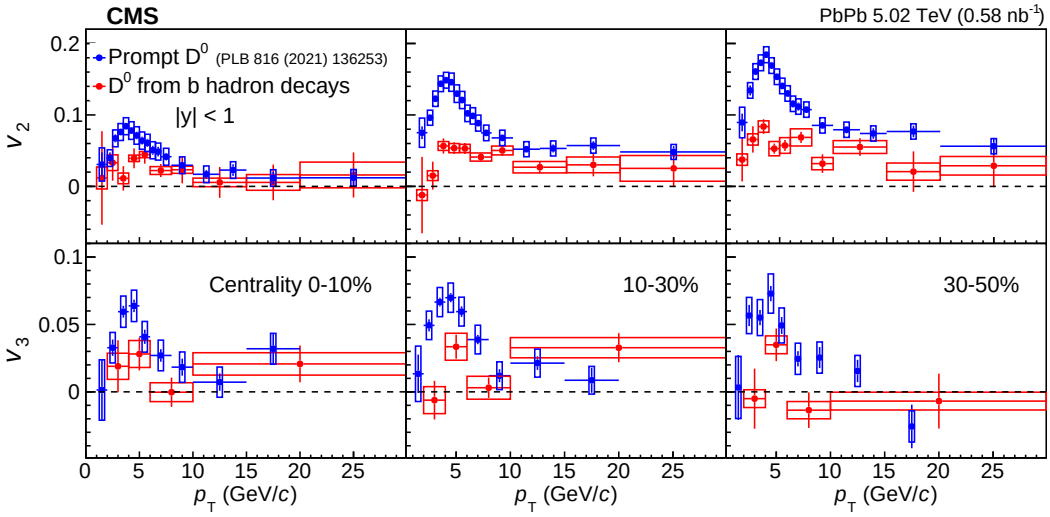

Figure 2: The elliptic, v_2 (upper panels), and the triangular, v_3 (lower panels), flow coefficients of nonprompt and prompt (from Ref. [18]) D^0 mesons as functions of their p_T and in three bins of centrality. The bars and the boxes represent statistical and systematic uncertainties, respectively.

flow signal is weaker for nonprompt than for prompt D^0 mesons, but the difference is not as large as that for the elliptic flow. Measurements of b hadrons decaying into D^0 mesons suggest positive v_3 for D^0 mesons of $p_T \sim 5\,\text{GeV}/c$. The ATLAS Collaboration v_3 results for b hadrons decaying into muons with $p_T > 4\,\text{GeV}/c$ were found to be consistent with zero [19].

Figure 3 shows the measured nonprompt D^0 meson v_n coefficients compared with theoretical calculations that have different modeling of the b quark flow. The PHSD model is a microscopic off-shell transport model based on a Boltzmann transport equation approach, and includes only collisional energy loss [49]. The TAMU model computes the space-time evolution of the heavy-quark phase space distribution in the QGP using the Fokker–Planck equation, implemented via Langevin dynamics, and also has no radiative energy loss [52]. The LGR model uses the Langevin approach with gluon radiation, emphasizing the in-medium diffusion dynamics. This model is best for describing heavy-quark evolutions from low to intermediate p_T range, $p_T < 15\,\text{GeV}/c$ [53, 54]. The LBT model is based on a linearized Boltzmann approach coupled to a hydrodynamic background, and employs both collisional and radiative energy loss [50, 51]. The CUJET3.0 is essentially a jet energy loss framework based on a nonperturbative QGP medium [55, 56]. The LBT and CUJET3.0 approaches are applicable only for the high-p_T range and do not have predictions for lower momenta. While all models can qualitatively describe the p_T dependence of the data, the LGR model reproduces the measurements for the centrality 30–50% and in the low- and the intermediate-p_T ranges, where b quarks follow Brownian motion, i.e., small random momentum fluctuations caused by collisions with thermal particles. For the central events, 0–10%, this model shows almost no p_T dependence and does not predict the peak structure seen in the data. In the same p_T range, the PHSD model provides a good description of the data, for centralities 0–10 and 10–30%, but it cannot describe the data at higher centralities. In contrast, this same PHSD model underpredicts the v_2 Fourier coefficients for D^0 mesons, which are not the product of b hadron decays [18]. The TAMU model has predictions in the centrality range 20–40%, therefore only an indirect comparison with data is possible, but the predictions describe well the measurement performed in the centrality range 10–30%. At higher p_T, where the anisotropy is driven by the path-length

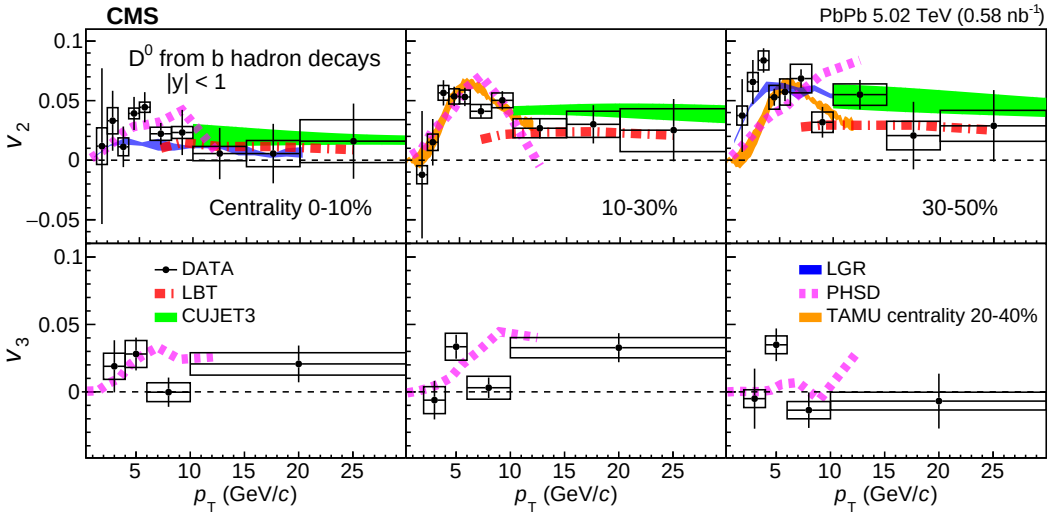

Figure 3: The elliptic, v_2 (upper panel), and the triangular, v_3 (lower panel), flow coefficients of nonprompt D^0 mesons as functions of their p_T and in three bins of centrality. The bars and the boxes represent statistical and systematic uncertainties, respectively. The colored bands show theoretical predictions [49–56].

dependence of parton energy loss, the LBT model gives lower predictions than CUJET3.0, but both models match data within uncertainties. The PHSD, LBT, and LGR models account for event-by-event fluctuations of the initial geometry, but PHSD is the only model that has predictions for v_3 coefficients. While precision is limited for both model and data, they reach similar maximal values in all centralities, with the exception that PHSD predicts the location of the maximum flow at a higher p_T than seen in data.

6 Summary

In summary, the elliptic (v_2) and triangular (v_3) flow harmonics of D^0 mesons that originate in b hadron decays (nonprompt D^0 mesons) are measured in lead-lead collisions at $\sqrt{s_\mathrm{NN}} = 5.02\,\mathrm{TeV}$. The v_2 results show a weak transverse momentum (p_T) dependence and suggest a slight increase for more peripheral collisions. An indication of a nonzero v_3 coefficient is found for nonprompt D^0 mesons with $4 < p_\mathrm{T} < 6\,\mathrm{GeV}/c$. The magnitudes of the flow coefficients are lower for nonprompt D^0 than for prompt D^0 mesons. This magnitude difference is more pronounced in the case of v_2. Comparisons of the results to theoretical models suggest a mass hierarchy in quark interactions with the quark-gluon plasma, thereby extending our understanding of heavy quark interactions with the medium.

References

[1] BRAHMS Collaboration, "Quark-gluon plasma and color glass condensate at RHIC? The perspective from the BRAHMS experiment", *Nucl. Phys. A* **757** (2005) 1, doi:10.1016/j.nuclphysa.2005.02.130, arXiv:nucl-ex/0410020.

[2] PHOBOS Collaboration, "The PHOBOS perspective on discoveries at RHIC", *Nucl. Phys. A* **757** (2005) 28, doi:10.1016/j.nuclphysa.2005.03.084, arXiv:nucl-ex/0410022.

[3] STAR Collaboration, "Experimental and theoretical challenges in the search for the quark-gluon plasma: the STAR Collaboration's critical assessment of the evidence from RHIC collisions", *Nucl. Phys. A* **757** (2005) 102, doi:10.1016/j.nuclphysa.2005.03.085, arXiv:nucl-ex/0501009.

[4] PHENIX Collaboration, "Formation of dense partonic matter in relativistic nucleus-nucleus collisions at RHIC: experimental evaluation by the PHENIX Collaboration", *Nucl. Phys. A* **757** (2005) 184, doi:10.1016/j.nuclphysa.2005.03.086, arXiv:nucl-ex/0410003.

[5] S. A. Voloshin and Y. Zhang, "Flow study in relativistic nuclear collisions by fourier expansion of azimuthal particle distributions", *Z. Phys. C* **70** (1996) 665, doi:10.1007/s002880050141, arXiv:hep-ph/9407282.

[6] W. Busza, K. Rajagopal, and W. van der Schee, "Heavy ion collisions: the big picture, and the big questions", *Ann. Rev. Nucl. Part. Sci.* **68** (2018) 339, doi:10.1146/annurev-nucl-101917-020852, arXiv:1802.04801.

[7] J.-Y. Ollitrault, "Anisotropy as a signature of transverse collective flow", *Phys. Rev. D* **46** (1992) 229, doi:10.1103/PhysRevD.46.229.

[8] U. Heinz and R. Snellings, "Collective flow and viscosity in relativistic heavy-ion collisions", *Ann. Rev. Nucl. Part. Sci.* **63** (2013) 123, doi:10.1146/annurev-nucl-102212-170540, arXiv:1301.2826.

[9] C. Gale, S. Jeon, and B. Schenke, "Hydrodynamic modeling of heavy-ion collisions", *Int. J. Mod. Phys. A* **28** (2013) 1340011, doi:10.1142/S0217751X13400113, arXiv:1301.5893.

[10] B. Alver and G. Roland, "Collision-geometry fluctuations and triangular flow in heavy-ion collisions", *Phys. Rev. C* **81** (2010) 054905, doi:10.1103/PhysRevC.81.054905, arXiv:1003.0194.

[11] F. Prino and R. Rapp, "Open heavy flavor in QCD matter and in nuclear collisions", *J. Phys. G* **43** (2016) 093002, doi:10.1088/0954-3899/43/9/093002, arXiv:1603.00529.

[12] R. Rapp et al., "Extraction of heavy-flavor transport coefficients in QCD matter", *Nucl. Phys. A* **979** (2018) 21, doi:10.1016/j.nuclphysa.2018.09.002, arXiv:1803.03824.

[13] H. van Hees, V. Greco, and R. Rapp, "Heavy-quark probes of the quark-gluon plasma and interpretation of recent data taken at the BNL Relativistic Heavy Ion Collider", *Phys. Rev. C* **73** (2006) 034913, doi:10.1103/PhysRevC.73.034913, arXiv:nucl-th/0508055.

[14] M. Gyulassy, I. Vitev, and X.-N. Wang, "High p_{T} azimuthal asymmetry in noncentral $A + A$ at RHIC", *Phys. Rev. Lett.* **86** (2001) 2537, doi:10.1103/PhysRevLett.86.2537, arXiv:nucl-th/0012092.

[15] E. V. Shuryak, "Azimuthal asymmetry at large p_{T} seem to be too large for a pure "jet quenching"", *Phys. Rev. C* **66** (2002) 027902, doi:10.1103/PhysRevC.66.027902, arXiv:nucl-th/0112042.

[16] ALICE Collaboration, "D-meson azimuthal anisotropy in midcentral Pb-Pb collisions at $\sqrt{s_{\mathrm{NN}}} = 5.02\,\mathrm{TeV}$", *Phys. Rev. Lett.* **120** (2018) 102301, doi:10.1103/PhysRevLett.120.102301, arXiv:1707.01005.

[17] CMS Collaboration, "Measurement of prompt D^0 meson azimuthal anisotropy in Pb-Pb collisions at $\sqrt{s_{\mathrm{NN}}} = 5.02\,\mathrm{TeV}$", *Phys. Rev. Lett.* **120** (2018) 202301, doi:10.1103/PhysRevLett.120.202301, arXiv:1708.03497.

[18] CMS Collaboration, "Measurement of prompt D^0 and $\overline{\mathrm{D}}^0$ meson azimuthal anisotropy and search for strong electric fields in PbPb collisions at $\sqrt{s_{\mathrm{NN}}} = 5.02\,\mathrm{TeV}$", *Phys. Lett. B* **816** (2021) 136253, doi:10.1016/j.physletb.2021.136253, arXiv:2009.12628.

[19] ATLAS Collaboration, "Measurement of azimuthal anisotropy of muons from charm and bottom hadrons in Pb+Pb collisions at $\sqrt{s_{\mathrm{NN}}} = 5.02\,\mathrm{TeV}$ with the ATLAS detector", *Phys. Lett. B* **807** (2020) 135595, doi:10.1016/j.physletb.2020.135595, arXiv:2003.03565.

[20] ALICE Collaboration, "J/ψ elliptic and triangular flow in Pb-Pb collisions at $\sqrt{s_{\mathrm{NN}}} = 5.02\,\mathrm{TeV}$", *JHEP* **10** (2020) 141, doi:10.1007/JHEP10(2020)141, arXiv:2005.14518.

[21] CMS Collaboration, "Probing charm quark dynamics via multiparticle correlations in PbPb collisions at $\sqrt{s_{\mathrm{NN}}} = 5.02\,\mathrm{TeV}$", *Phys. Rev. Lett.* **129** (2022) 022001, doi:10.1103/PhysRevLett.129.022001, arXiv:2112.12236.

[22] CMS Collaboration, "Suppression and azimuthal anisotropy of prompt and nonprompt J/ψ production in PbPb collisions at $\sqrt{s_{\mathrm{NN}}} = 2.76\,\mathrm{TeV}$", *Eur. Phys. J. C* **77** (2017) 252, doi:10.1140/epjc/s10052-017-4781-1, arXiv:1610.00613.

[23] ALICE Collaboration, "Elliptic flow of electrons from beauty-hadron decays in Pb-Pb collisions at $\sqrt{s_{\mathrm{NN}}} = 5.02\,\mathrm{TeV}$", *Phys. Rev. Lett.* **126** (2021) 162001, doi:10.1103/PhysRevLett.126.162001, arXiv:2005.11130.

[24] HEPData record for this analysis, 2022. doi:10.17182/hepdata.131598.

[25] CMS Collaboration, "The CMS experiment at the CERN LHC", *JINST* **03** (2008) S08004, doi:10.1088/1748-0221/3/08/S08004.

[26] CMS Collaboration, "Performance of the CMS level-1 trigger in proton-proton collisions at $\sqrt{s} = 13\,\mathrm{TeV}$", *JINST* **15** (2020) P10017, doi:10.1088/1748-0221/15/10/P10017, arXiv:2006.10165.

[27] CMS Collaboration, "The CMS trigger system", *JINST* **12** (2017) P01020, doi:10.1088/1748-0221/12/01/P01020, arXiv:1609.02366.

[28] CMS Collaboration, "Electron and photon reconstruction and identification with the CMS experiment at the CERN LHC", *JINST* **16** (2021) P05014, doi:10.1088/1748-0221/16/05/P05014, arXiv:2012.06888.

[29] CMS Collaboration, "Performance of the CMS muon detector and muon reconstruction with proton-proton collisions at $\sqrt{s} = 13\,\mathrm{TeV}$", *JINST* **13** (2018) P06015, doi:10.1088/1748-0221/13/06/P06015, arXiv:1804.04528.

[30] CMS Collaboration, "Description and performance of track and primary-vertex reconstruction with the CMS tracker", *JINST* **9** (2014) P10009, doi:10.1088/1748-0221/9/10/P10009, arXiv:1405.6569.

[31] CMS Collaboration, "Particle-flow reconstruction and global event description with the CMS detector", *JINST* **12** (2017) P10003, doi:10.1088/1748-0221/12/10/P10003, arXiv:1706.04965.

[32] CMS Collaboration, "Observation and studies of jet quenching in PbPb collisions at $\sqrt{s_{\mathrm{NN}}} = 2.76$ TeV", *Phys. Rev. C* **84** (2011) 024906, doi:10.1103/PhysRevC.84.024906, arXiv:1102.1957.

[33] CMS Collaboration, "Precision luminosity measurement in proton-proton collisions at $\sqrt{s} = 13$ TeV in 2015 and 2016 at CMS", *Eur. Phys. J. C* **81** (2021) 800, doi:10.1140/epjc/s10052-021-09538-2, arXiv:2104.01927.

[34] CMS Collaboration, "CMS luminosity measurement using nucleus-nucleus collisions at $\sqrt{s_{\mathrm{NN}}} = 5.02$ TeV in 2018", CMS Physics Analysis Summary CMS-PAS-LUM-18-001, 2022.

[35] CMS Collaboration, "Charged-particle nuclear modification factors in PbPb and pPb collisions at $\sqrt{s_{\mathrm{NN}}} = 5.02$ TeV", *JHEP* **04** (2017) 039, doi:10.1007/JHEP04(2017)039, arXiv:1611.01664.

[36] T. Sjöstrand et al., "An introduction to PYTHIA 8.2", *Comput. Phys. Commun.* **191** (2015) 159, doi:10.1016/j.cpc.2015.01.024, arXiv:1410.3012.

[37] CMS Collaboration, "Extraction and validation of a new set of CMS PYTHIA8 tunes from underlying-event measurements", *Eur. Phys. J. C* **80** (2020) 4, doi:10.1140/epjc/s10052-019-7499-4, arXiv:1903.12179.

[38] D. J. Lange, "The EVTGEN particle decay simulation package", *Nucl. Instrum. Meth. A* **462** (2001) 152, doi:10.1016/S0168-9002(01)00089-4.

[39] I. P. Lokhtin and A. M. Snigirev, "A model of jet quenching in ultrarelativistic heavy ion collisions and high-p_{T} hadron spectra at RHIC", *Eur. Phys. J. C* **45** (2006) 211, doi:10.1140/epjc/s2005-02426-3, arXiv:hep-ph/0506189.

[40] GEANT4 Collaboration, "GEANT4—a simulation toolkit", *Nucl. Instrum. Meth. A* **506** (2003) 250, doi:10.1016/S0168-9002(03)01368-8.

[41] Particle Data Group Collaboration, "Review of particle physics", *Prog. Theor. Exp. Phys.* **2022** (2022) 083C01, doi:10.1093/ptep/ptac097.

[42] H. Voss, A. Höcker, J. Stelzer, and F. Tegenfeldt, "TMVA, the toolkit for multivariate data analysis with ROOT", in *XIth International Workshop on Advanced Computing and Analysis Techniques in Physics Research (ACAT)*, p. 40. 2007. arXiv:physics/0703039. [PoS(ACAT)040]. doi:10.22323/1.050.0040.

[43] STAR Collaboration, "Elliptic flow from two- and four-particle correlations in Au + Au collisions at $\sqrt{s_{\mathrm{NN}}} = 130$ GeV", *Phys. Rev. C* **66** (2002) 034904, doi:10.1103/PhysRevC.66.034904, arXiv:nucl-ex/0206001.

[44] A. M. Poskanzer and S. A. Voloshin, "Methods for analyzing anisotropic flow in relativistic nuclear collisions", *Phys. Rev. C* **58** (1998) 1671, doi:10.1103/PhysRevC.58.1671, arXiv:nucl-ex/9805001.

[45] NA49 Collaboration, "Directed and elliptic flow of charged pions and protons in Pb+Pb collisions at 40A and 158A GeV", *Phys. Rev. C* **68** (2003) 034903, doi:10.1103/PhysRevC.68.034903, arXiv:nucl-ex/0303001.

[46] M. J. Oreglia, "A study of the reactions $\psi' \to \gamma\gamma\psi$". PhD thesis, Stanford University, 1980. SLAC Report SLAC-R-236.

[47] CMS Collaboration, "Studies of charm and beauty hadron long-range correlations in pp and pPb collisions at LHC energies", *Phys. Lett. B* **813** (2021) 136036, doi:10.1016/j.physletb.2020.136036, arXiv:2009.07065.

[48] CMS Collaboration, "Studies of beauty suppression via nonprompt D^0 mesons in Pb-Pb collisions at $\sqrt{s_{NN}} = 5.02$ TeV", *Phys. Rev. Lett.* **123** (2019) 022001, doi:10.1103/PhysRevLett.123.022001, arXiv:1810.11102.

[49] T. Song et al., "Tomography of the quark-gluon plasma by charm quarks", *Phys. Rev. C* **92** (2015) 014910, doi:10.1103/PhysRevC.92.014910, arXiv:1503.03039.

[50] S. Cao, T. Luo, G.-Y. Qin, and X.-N. Wang, "Linearized Boltzmann transport model for jet propagation in the quark-gluon plasma: heavy quark evolution", *Phys. Rev. C* **94** (2016) 014909, doi:10.1103/PhysRevC.94.014909, arXiv:1605.06447.

[51] W.-J. Xing, S. Cao, G.-Y. Qin, and H. Xing, "Flavor hierarchy of jet quenching in relativistic heavy-ion collisions", *Phys. Lett. B* **805** (2020) 135424, doi:10.1016/j.physletb.2020.135424, arXiv:1906.00413.

[52] M. He, R. J. Fries, and R. Rapp, "Heavy flavor at the large hadron collider in a strong coupling approach", *Phys. Lett. B* **735** (2014) 445, doi:10.1016/j.physletb.2014.05.050, arXiv:1401.3817.

[53] S. Li, C. Wang, W. Renzhuo, and J. Liao, "Probing the transport properties of quark-gluon plasma via heavy-flavor Boltzmann and Langevin dynamics", *Phys. Rev. C* **99** (2019) 054909, doi:10.1103/PhysRevC.99.054909, arXiv:1901.04600.

[54] S. Li and J. Liao, "Data-driven extraction of heavy quark diffusion in quark-gluon plasma", *Eur. Phys. J. C* **80 7** (2020) 671, doi:10.1140/epjc/s10052-020-8243-9, arXiv:1912.08965.

[55] S. Shi, J. Liao, and M. Gyulassy, "Probing the color structure of the perfect QCD fluids via soft-hard-event-by-event azimuthal correlations", *Chin. Phys. C* **42** (2018) 104104, doi:10.1088/1674-1137/42/10/104104, arXiv:1804.01915.

[56] S. Shi, J. Liao, and M. Gyulassy, "Global constraints from RHIC and LHC on transport properties of QCD fluids in CUJET/CIBJET framework", *Chin. Phys. C* **43** (2019) 044101, doi:10.1088/1674-1137/43/4/044101, arXiv:1808.05461.